Different formation histories between the African and Pacific large low shear-wave velocity provinces as revealed by their water contents

Xiao-Yan Gu[1*], Piao-Yi Wang[2], Eero Hanski[3], Bertrand Moine[4], Takeshi Kuritani[5], Mitsuhiro Nakagawa[5], Qun-Ke Xia[1], Jia Liu[1], Huan Chen[1]

[1]Key Laboratory of Geoscience Big Data and Deep Resource of Zhejiang Province, School of Earth Sciences, Zhejiang University, Hangzhou 310027, China, [2]School of Earth and Space Sciences, University of Science and Technology of China, Hefei 230026, China, [3]Oulu Mining School, University of Oulu, P. O. Box 3000, 90014 Oulu, Finland, [4]Université de Lyon, UJM-Saint-Etienne, UCA, IRD, CNRS, Laboratoire Magmas et Volcans, UMR6524, Saint-Etienne, France, [5]Graduate School of Science, Hokkaido University 060-0810, Japan

*Corresponding authors. Email: gxy0823@zju.edu.cn (X.-Y. G.)

Key points:

- H_2O distribution in a single large low shear-wave velocity province is heterogeneous.
- The African large low shear-wave velocity province has higher H_2O content and H_2O/Ce than the Pacific large low shear-wave velocity province.
- The two large low shear-wave velocity provinces may have different formation and evolution histories.

Abstract

Global tomographic models have revealed the existence of two large low shear-wave velocity provinces (LLSVPs) underlying Africa and the Pacific, which are regarded as sources of most typical mantle plumes. Plume-induced basalts have the potential to imply the formation mechanisms and evolutional histories of the LLSVPs. In this study, we measured H_2O contents in clinopyroxene and olivine phenocrysts from Cenozoic basalts produced by the Kerguelen and Crozet mantle plumes, which are deeply rooted in the African LLSVP. The results were used to constrain the H_2O content in the source of basalts, yielding 1805 ± 579 ppm for the Kerguelen plume and 2144 ± 690 ppm for the Crozet plume. H_2O contents in the mantle sources of basalts fed by other plumes rooted in these two LLSVPs were calculated from literature data. Combining these results together, we show that the African LLSVP seems to have higher H_2O content and H_2O/Ce (620-2144 ppm and 184-592, respectively) than the Pacific LLSVP (262-671 ppm and 89-306, respectively). These features could be ascribed to incorporation of subducted material, which had experienced variable degrees of dehydration during its downwelling, into the LLSVPs. Our results imply that the continuous incorporation of subducted oceanic crust modifies the compositions of LLSVPs and induces heterogeneous distribution of H_2O within individual LLSVPs and distinct H_2O contents between the African and Pacific LLSVPs. This suggests that the African and Pacific LLSVPs might have different formation and evolution histories.

Plain language summary

Seismic tomography has revealed that large-scale heterogeneity exists at the base of the mantle, dominantly manifested by two large low shear-wave velocity provinces (LLSVPs) beneath Africa

and the Pacific. The LLSVP may play a key role in the global mantle convection and the core-mantle interaction, but their compositions and causes remain enigmatic up to present. Mantle plume-induced ocean island basalts (OIBs), originally related to the LLSVPs, can potentially supply some clues for this point. The presence of H_2O can remarkably influence the physical and chemical properties of mantle rocks. Moreover, H_2O contents and H_2O/Ce ratios in basalts are efficient tracers to characterize the basalt sources. We compiled and inversely estimated the source H_2O contents for global OIBs to track H_2O distribution in the LLSVPs. The distribution of H_2O shows significant heterogeneity both inside a single LLSVP and between the two LLSVPs. The incorporation of subducted oceanic crusts with variable dehydration extents during downwelling may be responsible for the heterogeneous H_2O distribution within individual LLSVPs and the distinct H_2O contents and H_2O/Ce ratios between the African and Pacific LLSVPs. It may also imply the different formation and evolutional histories for the two LLSVPs.

1. Introduction

Seismic tomography revealed large-scale heterogeneity at the base of the mantle, dominated by two large low shear-wave velocity provinces (LLSVPs), one beneath Africa and the other beneath the Pacific, with regions around the LLSVPs corresponding to an assembly of cooler subducted slabs (Cottaar & Lekic, 2016; Garnero et al., 2016). Up to the present, the formation mechanism and geochemical nature of the LLSVPs have remained controversial. Several lines of geophysical evidence support the view that LLSVPs have distinct compositional properties compared with the ambient mantle and can be regarded as thermochemical piles (e.g., Garnero et al., 2016). Two different hypotheses have been put forward to explain the origin of the piles: they are primordial features generated during an ancient differentiation event (e.g., Labrosse et al., 2007; Lee et al.,

2010) or they represent an assembly of subducted oceanic crust (e.g., Brandenburg & van Keken, 2007; Mulyukova et al., 2015; Thomson et al., 2019). Diverse seismic studies have delineated typical mantle plumes as fluxes of material and energy originating from the LLSVPs (e.g., French & Romanowicz, 2015; Marignier et al., 2020; Montelli et al., 2004, 2006). Hotspots have long been considered as surficial expressions of mantle plumes (Hofmann, 1997; White, 2015). Thus, hotspot-related basalts could potentially serve as windows to geochemical characteristics of the LLSVPs, further providing information on their formation and evolution (e.g., Doucet et al., 2020; Homrighausen et al., 2020; Huang et al., 2011; Jackson et al., 2018). Doucet et al. (2020) compiled Sr-Nd-Pb isotope data on plume-generated basalts from ocean islands and oceanic plateaus overlying geographically both the African and Pacific LLSVPs. They proposed that these two LLSVPs have distinct geochemical compositions and evolutionary histories.

Garnero et al. (2016) highlighted the significance of volatiles in the formation of LLSVPs and demonstrated that these two LLSVPs may have compositional differences induced by different influxes of volatiles and recycled materials. Indeed, the presence of H_2O can significantly affect the physical and chemical properties of mantle rocks under conditions of the lowermost mantle, including, for instance, melting processes (Nomura et al., 2014), viscosity (Nakagawa et al., 2015), and thermal conductivity (Hsieh et al., 2020). Different subducted slabs could undergo variable extents of dehydration during their subduction or residence in the deep mantle, suggesting that the continuous incorporation of subducted oceanic crust can potentially induce heterogeneous distribution of H_2O in the deep mantle (Dixon et al., 2002; Workman et al, 2006). Since diverse mantle components have distinct H_2O contents and H_2O behaves incompatibly during partial melting with a compatibility similar to that of Ce, H_2O contents and H_2O/Ce ratios of basalts have

been proposed as efficient tracers of compositional features for basalt sources (e.g., Dixon et al., 2002; Kendrick et al., 2017). Therefore, H_2O contents and H_2O/Ce ratios of LLSVP-derived plumes can give new insights into the formation and evolution of LLSVPs. However, so far, no comparison of the H_2O contents between the Africa and Pacific LLSVPs has been undertaken.

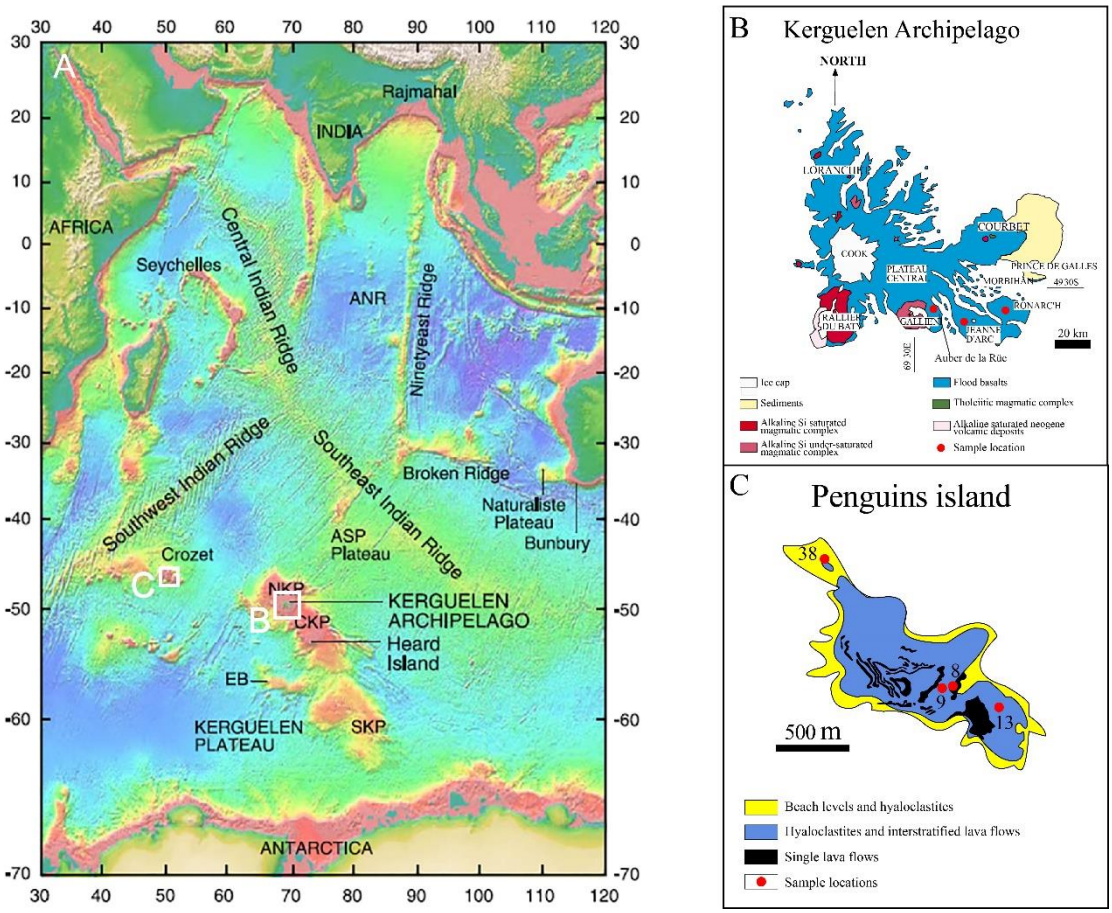

Figure 1 Bathymetric map of the Indian Ocean (A) modified from Doucet et al. (2005), with the locations of the studied Kerguelen basalts from the Kerguelen Archipelago (B) and Crozet basalts from the Penguins Island (C). Kerguelen basalts with an age of less than 25 Ma were sampled during several field missions in the southeast Kerguelen Archipelago.

In this study, we provide new H_2O abundance data in primary melts of Cenozoic basalts from the Kerguelen and Crozet Archipelagos (Figure 1), which have been suggested to originate from the Africa LLSVP. And we also compile H_2O contents reported previously for diverse plume-related oceanic island basalts (OIBs) associated with the two LLSVPs. The large variations in the estimated

95 H_2O contents and H_2O/Ce ratios in the mantle sources of OIBs imply that recycled materials
96 advected into the LLSVPs might have experienced dehydration to various degrees during their
97 subduction or storage in the deep mantle. Higher H_2O contents and H_2O/Ce ratios in the African
98 LLSVP than in the Pacific LLSVP are suggestive of distinct formation or evolution histories for
99 these LLSVPs.

100 **2. Geological background**

101 The Kerguelen mantle plume has produced magmatic activity since ~130 Ma, generating the
102 Kerguelen-Broken Ridge large igneous province and the Ninetyeast Ridge volcanic track with a
103 length of around 5000 km (Coffin et al., 2002; Frey et al., 2000a). Doucet et al. (2006) analyzed He
104 and Ne isotopic compositions of olivine phenocrysts from picrites and high-MgO basalts collected
105 from the same regions and having the same eruption ages as the basaltic samples investigated in this
106 study. They confirmed that the Kerguelen mantle plume entrained primitive material from the deep
107 mantle (R/R_a = 8-18; average $^{21}Ne/^{22}Ne$ = 0.044 after correction for air contamination). Basalts of
108 the Crozet mantle plume have resulted in a series of islands located in the Indian Ocean. Breton et
109 al. (2013) reported major and trace element data and Sr-Nd-Pb-He isotopic compositions for Crozet
110 plume-related basalts and demonstrated that the plume source is heterogeneous in composition and
111 represents a mixture of two or three endmembers. Four samples from the Penguins Island with
112 primitive He isotopic compositions (R/R_a = 13.19-13.98; Breton et al., 2013) were selected for this
113 study. Geophysical observations indicated that the Kerguelen and Crozet mantle plumes are rooted
114 in the African LLSVP (French & Romanowicz, 2015; Montelli et al., 2006). More detailed
115 description of the geological background and petrological features of the studied samples are given
116 in the supporting information.

3. Analytical methods

Chemical compositions of bulk-rock samples were obtained using X-Ray fluorescence spectrometry and inductively coupled plasma mass spectrometry at ALS Chemex Co., Ltd. (Guangzhou, China). Fourier transform infrared spectroscopy (FTIR) was applied to measure H_2O contents of clinopyroxene (Cpx) phenocrysts under unpolarized radiation by a Nicolet iS50 FTIR attached to a Continuμm microscope at the School of Earth Sciences, Zhejiang University, China. The compositions of olivine and Cpx phenocrysts were analyzed by a Shimadzu electron probe microanalyzer (EPMA 1720) at the School of Earth Sciences, Zhejiang University, China. The concentrations of trace elements in Cpx phenocrysts were analyzed by the laser ablation inductively coupled plasma mass spectrometry (LA-ICPMS) at the School of Earth Sciences, Zhejiang University, China. Sr-Nd-Pb isotopic analyses were conducted using a multi-collector inductively coupled plasma mass spectrometer (MC–ICP–MS; Thermo Fisher Scientific Neptune Plus) at Hokkaido University, Japan. More details of the used analytical methods are reported in the supporting information.

4. Results

4.1. Bulk-rock compositions of Kerguelen and Crozet basalts

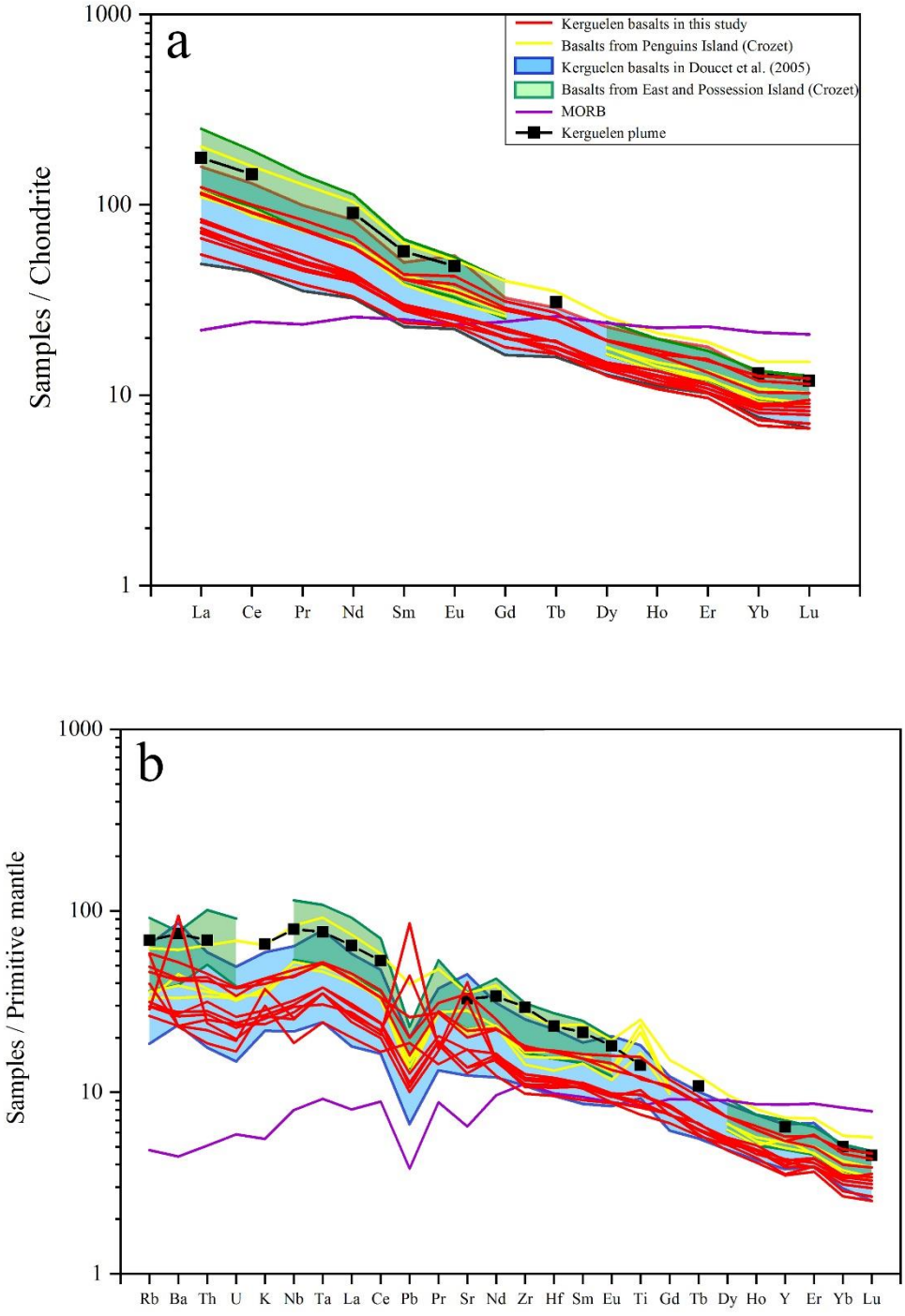

Figure 2 Chondrite-normalized rare earth element (REE) and primitive mantle-normalized trace element patterns for Crozet and Kerguelen basalts. The trace element compositions of the Crozet basalts are from Breton et al. (2013). Trace element compositions of high-MgO basalts and picrites studied by Doucet et al. (2005) are also

shown for comparison. The average trace element compositions of global MORB and basalts representing direct melting products of the Kerguelen plume are from Gale et al. (2013) and Frey et al. (2000b), respectively. Normalization values after McDonough and Sun (1995).

Major and minor element and Sr-Nd-Pb isotopic compositions of representative bulk-rock samples are shown in Tables S1-3. The selected samples display a porphyritic texture, with the phenocrysts being mainly olivine and Cpx. All the samples have loss-on-ignition values lower than 2.4 wt.% and MgO contents ranging from 7.1 to 20.0 wt.% (Table S1). The samples with high MgO contents have experienced olivine and/or Cpx accumulation as evidenced by the relationship between other major elements and MgO (Figure S2). All the samples show significant light rare earth elements (LREE) and large ion lithophile elements (LILE) enrichment and no negative Nb-Ta anomalies, as revealed by primitive mantle-normalized trace element patterns (Figures 2a, b). Their Nb/U ratios fall in the range of worldwide mid-ocean ridge basalts (MORBs) and OIBs, whereas several Kerguelen samples have lower Ce/Pb ratios, probably due to surficial alteration influencing the Pb concentrations in these samples (Figures S3a, b).

The Sr-Nd isotopic compositions of the studied Kerguelen basalts resemble those reported in previous studies, showing little variations and falling close to the EMI endmember (Figure 3a; White, 2015). For the Pb isotopic compositions, the studied samples form a trend mostly overlapping with earlier Kerguelen samples, but extending towards lower Pb isotopic ratios (Figure 3c). Similar trends have been ascribed by Doucet et al. (2005) to intrinsic compositional heterogeneity in the Kerguelen mantle plume. The Sr-Nd-Pb isotopic compositions of the Crozet basalts form two groups plotting away from the Kerguelen field towards the MORB fields in the Sr-Nd isotope diagram (Figure 3a) whereas in the Pb-Pb isotope diagram, they plot away from other fields due to their high

158 $^{206}Pb/^{204}Pb$ ratios. The samples selected for H_2O analysis from Crozet follow a trend extending

159 towards the HIMU endmember (Figures 3a, b, c; Breton et al., 2013).

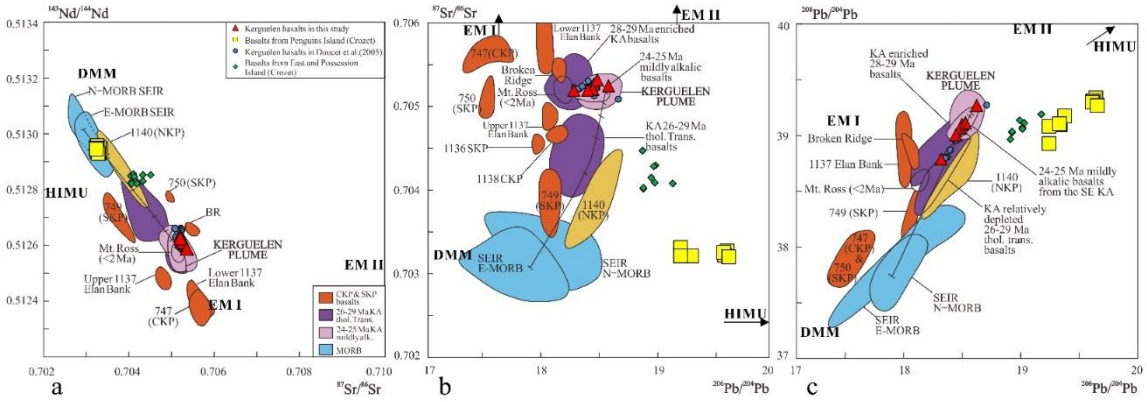

160 **Figure 3 Sr-Nd-Pb isotopic compositions of basalts from the Crozet and Kerguelen Archipelagos.** The data of

161 Crozet basalts (including from Penguins, East and Possession Islands) are adopted from Breton et al. (2013). The

162 Crozet basalts analyzed for H_2O in this study were sampled from the Penguins Island, and their sources have a

163 contribution from the HIMU component as indicated by the trend to high $^{206}Pb/^{204}Pb$ ratios (b and c). The fields of

164 SEIR MORBs and different basalts related to the Kerguelen plume, including those from the Southern Kerguelen

165 plateau (SKP), Central Kerguelen Plateau (CKP), Broken Ridge (BR), Elan Bank, NKP, etc., are based on data from

166 Doucet et al. (2005) and references therein. The basalts in the Kerguelen Archipelago display temporally

167 compositional variations, with basalts with an age higher than 25 Ma being more depleted due to contamination with

168 SEIR MORB. The fields representing isotopic compositions of the Kerguelen mantle plume are defined by the

169 compositions of basalts from Mt. Crozier (Doucet et al., 2005; Weis et al., 2002).

170 **4.2. H_2O contents in Cpx phenocrysts and equilibrated melts for Kerguelen and Crozet basalts**

171 Measured H_2O contents in Cpx phenocrysts and calculated H_2O contents in melts equilibrated with

172 individual Cpx phenocrysts, together with major element compositions of Cpx phenocrysts, are

173 reported in Dataset S1.

174 **4.2.1. Petrographic and geochemical characteristics of Cpx phenocrysts**

175 Most of the Cpx phenocrysts are euhedral and no major element diffusion zonation has been

176 observed in the backscattered electron images (Figure S4). The analyzed Cpx phenocrysts have Mg#

(=molar 100×Mg/(Mg+Fe)) values ranging from 74.1 to 88.7 and from 74.3 to 88.3 for the Kerguelen and Crozet basalts, respectively (Dataset S1). As mentioned in Section 4.1 and the precious studies (Doucet et al., 2005, 2006; Breton et al., 2013), some samples with high MgO contents should have experienced the olivine and/or Cpx accumulation, and the Cpx phenocrysts in several samples display Fe-Mg disequilibrium with the bulk rocks (Table S1 and Dataset S1). However, petrographic and geochemical characteristics suggest that these Cpx phenocrysts should have crystallized from the early batches of melts with similar compositions to the host magmas. Firstly, SiO_2, TiO_2 and Al_2O_3 contents display single co-relationship with Mg# (Figure S5). Secondly, different Cpx phenocrysts in a single sample show parallel REE patterns (Figure S6), which could be explained by the fractionation of magma. Thirdly, most of the Cpx are euhedral, without rounded or resorbed texture and obvious compositional zonation. We selected suitable Cpx phenocrysts that have crystallized from melts with similar characteristics with the host magmas, to retrieve the water content information of primary melts and sources for the Kerguelen and Crozet basalts.

4.2.2. Water contents in Cpx phenocrysts and their equilibrated melts

The infrared spectra of Cpx phenocrysts display typical structural OH absorption bands similar to mantle Cpx (Figure 4a). H_2O contents of Cpx phenocrysts were determined ranging from 74 to 89 and from 7 to 858 ppm, respectively (Dataset S1). The uncertainty for a single analysis by unpolarized FTIR was estimated to be less than 30% (Liu et al., 2015; Xia et al., 2013). H_2O partition coefficients between Cpx and melt were calculated from major element compositions of Cpx. These were combined with the obtained H_2O contents in Cpx to estimate H_2O contents in the melts in equilibrium with Cpx, yielding values ranging from 0.07 to 7.74 wt.% (Dataset S1). Taking into

account the errors in the H_2O content measurements and calculation of the H_2O partition coefficient values, we estimated that the uncertainty is about 32% for the estimation of the H_2O content in the melts equilibrated with Cpx phenocrysts (Liu et al., 2015).

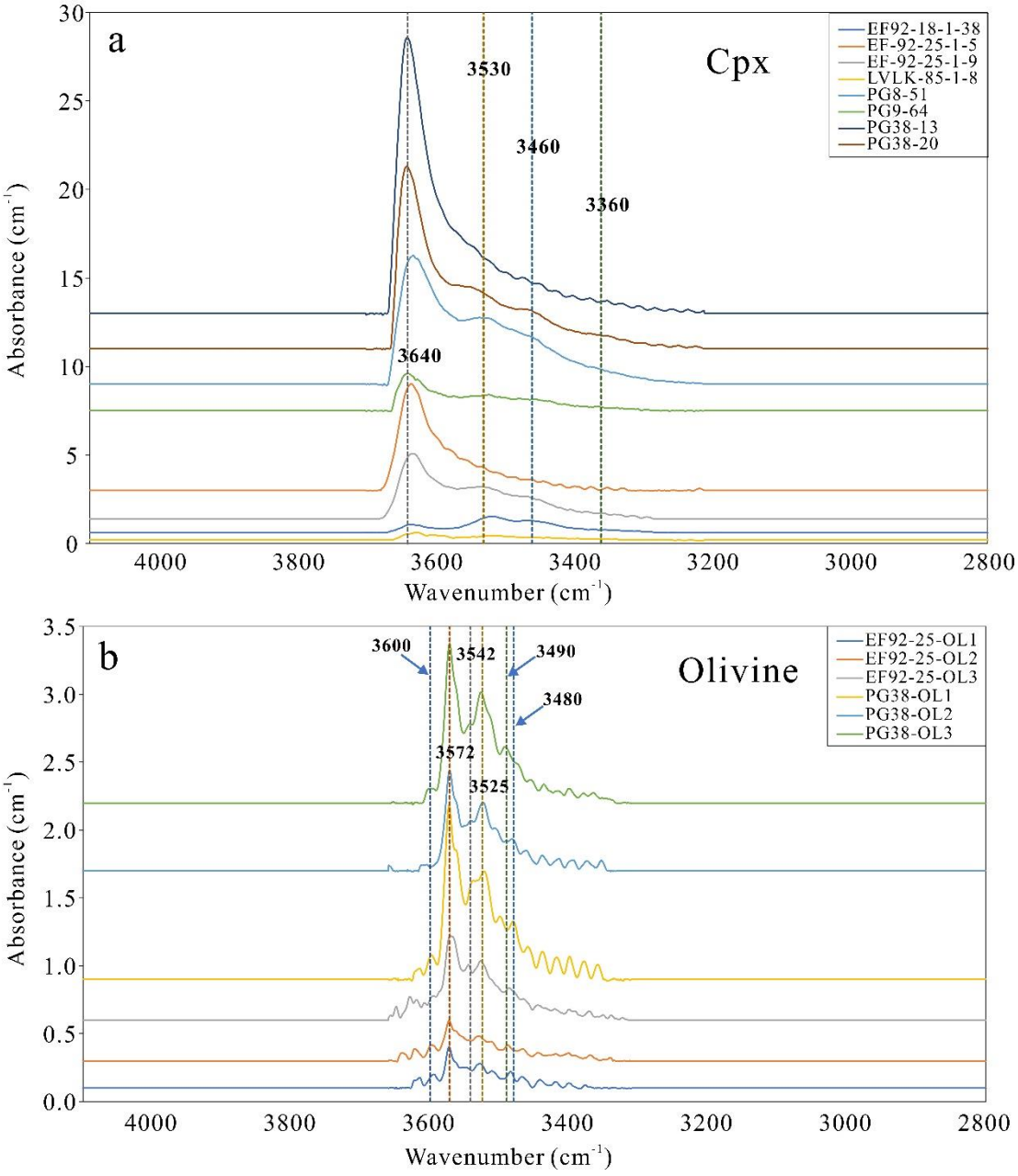

Figure 4 Representative infrared spectra for Cpx (a) and olivine (b) phenocrysts in Kerguelen and Crozet basalts. The spectra display main peaks of structural OH absorption at wavenumbers similar to those previously observed for mantle olivine and Cpx (marked by the dotted lines; e.g., Bell et al., 1995, 2003). The spectra are shown after baseline correction and absorbance normalization to the thickness of 1 cm.

4.3. Estimation of H_2O contents in the primary melts of Kerguelen and Crozet basalts

The H_2O contents in Cpx phenocrysts from the Kerguelen and Crozet basalts vary largely, which do not show any co-variation with Mg# of Cpx phenocrysts (Dataset S1; Figures S8a, b). This indicates that many Cpx phenocrysts in Kerguelen and Crozet basalts have more or less lost some of their initial H_2O due to decompression-induced degassing or diffusive loss during their ascent to the surface, which have been proposed to occur in Cpx from some island arc basalts and OIBs (Lloyd et al., 2016; Weis et al., 2015). Nevertheless, we still observed signatures suggesting that those Cpx phenocrysts with high water content likely did not experience significant overprinting, which can be applied to retrieve the lower bound of the H_2O contents in corresponding primary melts.

In the Kerguelen samples, some Cpx phenocrysts from sample EF92-25 deviate from the overall trend and have outstandingly high H_2O contents (e.g., >150 ppm; Figure S8a; Dataset S1). No observable differences in the OH band positions, band widths or peak heights are present in the spectra obtained by FTIR profile analyses for cores and rims of these Cpx phenocrysts. When the H_2O partition coefficient ($D_{Cpx/olivine}$) between Cpx and olivine in the basaltic system is considered to be 12.5 (Aubaud et al., 2004), olivine phenocrysts with 12.3-32.7 ppm H_2O in this sample (Figure 4b; Dataset S1) is close to equilibrium with those Cpx phenocrysts with high water contents (>150 ppm). Because hydrogen diffusivity in in olivine is one to two orders of magnitude faster than that in Cpx under high temperatures (e.g., >1250 ℃; Tian et al., 2017; Xu et al., 2019), the equilibrium distribution of water in Cpx and olivine indicates that these H_2O-enriched Cpx phenocrysts should have preserved their initial H_2O contents during the eruption and cooling process.

The similar observations to the Kerguelen case are also present for Crozet samples. Cpx phenocrysts in sample OVPG38 have high H_2O contents at given high Mg# (311-858 ppm for Cpx phenocrysts with Mg# from 81.9 to 88.3, respectively; Dataset S1; Figure S8b). Several lines of evidence support

229 that the Cpx phenocrysts in this sample have preserved their initial H_2O contents: the profile
230 analyses unraveled no core-to-rim H_2O content variations; H_2O contents correlates positively with
231 Al_2O_3 and TiO_2 contents in Cpx phenocrysts (Figures S9a, b). Moreover, olivine phenocrysts in this
232 sample have H_2O concentrations of 22.5-62.3 ppm (Fig. 4b; Dataset S1), rightly in equilibrium with
233 the coexisting Cpx phenocrysts. In several olivine phenocrysts, the FTIR profile analyses revealed
234 that the H_2O contents display homogeneous plateaus and steep decrease when approaching grain
235 boundaries (Figure S10).

236 The high water contents coexisting in the cores of Cpx and olivine phenocrysts would be explained
237 by the assimilation of some altered/hydrated crusts in the deep magma chamber before the eruption.
238 However, the geochemical characteristics of the Cpx phenocrysts do not support this possibility. As
239 shown in Figure S5, the Cpx phenocrysts with both high and low water contents show parallel REE
240 patterns which is consistent with the simple fractional crystallization trend from batches of magmas
241 originating from the same primary melt. In addition, if the measured high water content had been
242 brought by the assimilated altered crust, Ce/Pb ratios should decrease in accompany with the
243 increase of water contents in the Cpx phenocrysts. There is no clear trend between the Ce/Pb ratio
244 and water content in Cpx phenocrysts (Figure S9c). Finally, the calculated water content in the
245 equilibrated melt is as high as ~7.7 wt.%, requiring the exotic contaminated materials have much
246 higher water contents, which is hard to meet for the usual alteration process in the oceanic crust.
247 Overall, we suggest that the high water contents of those Cpx phenocrysts could be used to infer
248 water content of the primary melt.

249 The average H_2O contents in the Cpx phenocrysts that have preserved their initial H_2O are 220.8 ±
250 33.6 ppm and 519.6 ± 117.2 ppm for the Kerguelen and Crozet samples, respectively, while the

average H_2O contents in equilibrated melts are 2.02 wt.% and 3.97 wt.%. To decrease the errors of the estimated H_2O contents in primary melts, only Cpx phenocrysts with Mg# higher than 85 were taken into consideration for the estimation of H_2O contents in primary melts. The compositions of primary melts were established by incremental addition of olivine to the bulk-rock compositions until Mg# of equilibrated olivine equaled 90.0. Based on the average amount of olivine addition, the H_2O contents in the primary melts of the Kerguelen and Crozet basalts can be estimated to be 1.68 ± 0.54 wt.% and 3.69 ± 1.18 wt.%, respectively. The detailed calculation procedure is described in the supporting information.

5. Discussion

5.1. Potential contamination by depleted upper mantle material?

During ascending to the surface, basalts might undergo magma mixing and contamination with adjacent rocks. These processes could cause their compositions to deviate from the primary melts and thus make the estimation of the compositional nature of their sources more complex. To access the geochemical characteristics of mantle plumes, basalts representing direct melting products of plumes should be explored. The previous study has demonstrated that the Crozet basalts selected for this study have not experienced magma mixing and contamination by the Indian oceanic lithosphere (Breton et al., 2013) and can be used to evaluate the H_2O content in the Crozet mantle plume.

No evidence has been found to support the presence of a continental component in Cenozoic basalts from the Northern Kerguelen Plateau (NKP), including the Kerguelen Archipelago (e.g., Doucet et al., 2005; Weis & Frey, 2002). However, the compositions of submarine basalts from the NKP and

older (>25 Ma) basalts in the Kerguelen Archipelago display a depletion trend towards the Southeast Indian Ridge (SEIR) MORB. This has been interpreted as the result of the interaction between the Kerguelen mantle plume and the SEIR MORB source mantle (Doucet et al., 2005; Frey et al., 2000a; Weis & Frey, 2002). As the SEIR migrated far away from the plume (>400 km) after 25 Ma, contamination with depleted upper mantle material is not reflected in the compositions of Kerguelen basalts, but they exclusively represent geochemical characteristics of the Kerguelen mantle plume itself (Doucet et al., 2005). For the studied samples, the primitive mantle-normalized trace element patterns are similar to those of the inferred enriched component of the Kerguelen plume (Figure 2). Doucet et al. (2005) observed that the Nb/Zr ratio can be used as a good indicator to distinguish basalts contaminated with depleted upper mantle (≤0.1) from those produced by direct melting of the Kerguelen mantle plume (≈0.15; Figure S11). The Nb/Zr ratios of ~0.12-0.17 in our samples suggest that the compositions of these basalts have not been influenced by materials from the depleted upper mantle. Moreover, the Sr-Nd isotopic compositions of the studied samples exhibit little variability and fall in the range of basalts from Mt. Crozier, which have been proposed to be the best representatives of the compositions of the Kerguelen mantle plume (Figure 3a; Weis et al., 2002). In summary, trace element and Sr-Nd-Pb isotopic compositions indicate that, excluding fractional crystallization, the samples studied here can be regarded as unmodified melting products of the Kerguelen mantle plume.

5.2. Comparison with previous estimations of H_2O contents in the Kerguelen basalts

H_2O contents in basalts originally related to the Kerguelen mantle plume have previously been estimated using unaltered glasses recovered from submarine pillow basalts from the NKP (Wallace, 2002). These estimates (0.25-0.69 wt.%) are much lower than that (1.68 ± 0.54 wt.%) obtained in

this study for the primary melts of the Kerguelen mantle plume. It is worth noting that trace element and Sr-Nd-Pb isotopic compositions of glasses indicate mixing of components from the depleted SEIR MORB source mantle into the Kerguelen mantle plume (Weis & Frey, 2002). Moreover, the measured H_2O contents increase from 0.25-0.27 wt.% in glasses with 90-99% of the depleted component to 0.69 wt.% in enriched glasses with 63-76% of the depleted component (Wallace, 2002; Weis & Frey, 2002). This means that the Kerguelen mantle plume, as an enriched endmember, should contain more H_2O and produce primary melts with higher H_2O contents than the enriched glasses analyzed by Wallace (2002). Based on our estimation, a binary mixing model can simulate the H_2O contents in the enriched glasses from the NKP. This model involves a SEIR MORB-like melt and a primary melt from the Kerguelen mantle plume as the two end-members and yields mixing proportions similar to those obtained from Sr-Nd isotopic compositions (Figure S12; Weis & Frey, 2002). Thus, our estimation from Cpx phenocrysts should be reliable in assessing the H_2O content in the primary melt of the Kerguelen mantle plume.

No previous studies have been conducted to probe the H_2O contents of the Crozet basalts. Otherwise, the interaction of the Crozet plume with the segment of the Southwest Indian Ridge between the Indomed and Gallieni transform faults has been confirmed by geophysical and geochemical studies (Breton et al., 2013; Sauter et al., 2009). H_2O contents in the primary melts of basalts sampled from that segment were estimated to be 1.3 ± 0.3 wt.% and the H_2O/Ce ratios are higher than 1670, being much higher than H_2O/Ce in normal MORBs (Li et al., 2017). This observation indicates that the mantle source of the Crozet plume is enriched in H_2O, which is consistent with our results.

5.3. H_2O contents in primary melts and mantle sources of global plume-related OIBs

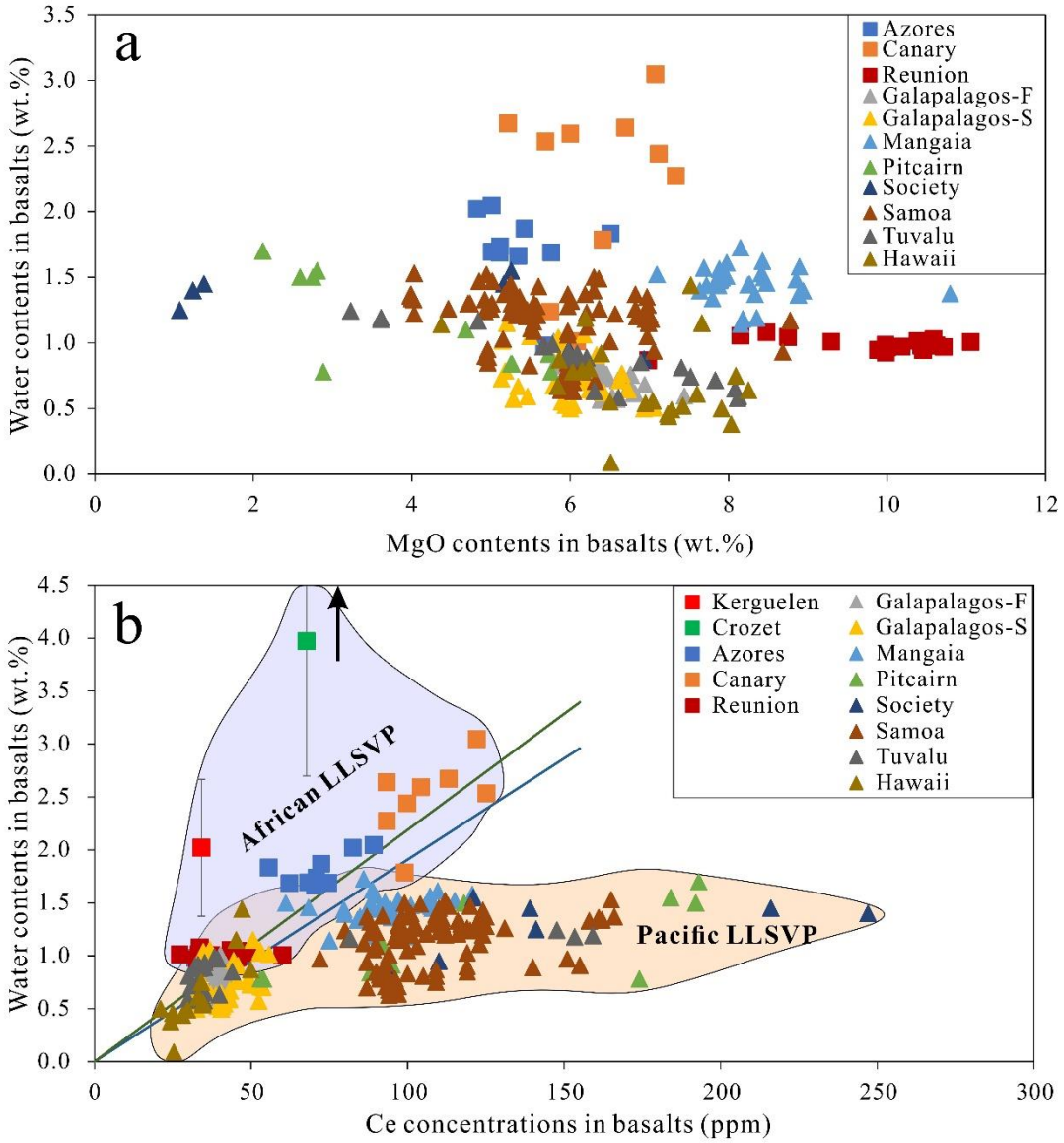

Figure 5 H_2O abundances of plumed-related OIBs reported in previous studies, plotted against MgO contents (a) and Ce concentrations (b). H_2O data of basalts affected by later processes (e.g., decompression-induced degassing, diffusive H gain, shallow alteration) were omitted. While basalts from the Azores, Canary and Mangaia hotspots have higher H_2O for the same MgO content, basalts from other hotspots form an overall trend with negative correlation between H_2O and MgO produced by fractional crystallization (a). In panel b, H_2O contents vary with Ce concentrations along different trends when the hotspots originally related to the Pacific (labelled by triangles) and African (labelled by squares) LLSVPs are compared. The DMM-FOZO trend defined by the H_2O-Ce relations in global MORBs and FOZO OIBs is shown as black lines (Shimizu et al., 2019). For the Galapalago hotspot, only H_2O contents in basalts with $^3He/^4He$ >8 were taken into consideration (two groups Fernandina and Sierra Negra,

suffixed by 'F' and 'S'; Peterson et al., 2017). The estimated H_2O and Ce contents in primary melts of the Kerguelen and Crozet basalts are also shown in panel b. Data sources are: Azores (Métrich et al., 2014), Canary (Longpré et al., 2017), Reunion (Walowski et al., 2019), Galapagos (Peterson et al., 2017), Mangaia (Cabral et al., 2014), Pitcairn (Kendrick et al., 2014), Society (Kendrick et al., 2014), Samoa (Workman et al., 2006; Kendrick et al., 2015), Tuvalu (Jackson et al., 2015) and Hawaii (Dixon & Clague, 2001; Shimizu et al., 2019).

We compiled H_2O content data previously reported for many hotspot-related OIBs. These hotspots have been explicitly evidenced by geophysical observations to overlie mantle plumes and are geographically associated with the two LLSVPs (Dataset S2; Figure 5a; Jackson et al., 2018). Results from some melt inclusions or glasses, disturbed by later processes (decompression-induced degassing, diffusive H gain, surficial alteration, etc.), were not taken into consideration (the detail of data infiltration discussed in the supporting information). It is noteworthy that the melt inclusions and basaltic glasses used in previous studies to explore the H_2O contents of diverse OIBs have mostly relatively low MgO contents (many lower than 6 wt.%; Dataset S2; Figure 5a). Additionally, the broad negative correlation between H_2O and MgO contents indicates that the H_2O inventory in the parental melts of these OIBs have been modified by fractional crystallization processes in variable extents (Figure 5a). To estimate the H_2O distribution in the LLSVPs, H_2O contents in primary melts of individual OIBs were roughly retrieved by incremental addition of equilibrium olivine to the bulk-rock compositions. As fractional crystallization in variable extents occurred to melts of OIBs, the compositions of melt inclusions and glasses, with highest MgO contents studied for H_2O contents of individual OIBs, were applied for the initial compositions for olivine addition. Assuming that H_2O behaves completely incompatibly during olivine fractionation, the primary H_2O contents were back calculated (cf. Le Voyer et al., 2015). With the assumption of melting degrees of 5% for alkali OIBs and 10% for tholeiites, we estimated the H_2O contents in the mantle sources

using the batch and fractional partial melting models (Shaw, 1970). A detailed calculation procedure and results are shown in the supporting information and Table 1. The calculated H_2O contents in the primary melts and mantle sources display great variations for OIBs associated with a single LLSVP and large differences between OIBs associated with the African and Pacific LLSVPs (Table 1; Figure 6a).

As the transition zone is a significant H_2O reservoir along the ascent route of deep mantle-rooted plumes, variable amounts of transition zone materials captured in ascending plumes may be a plausible mechanism to induce heterogeneous H_2O contents in distinct plume-related OIBs. When traversing the transition zone, Archean plumes had higher mantle potential temperatures, causing them to partially melt and potentially take in H_2O from the transition zone, whereas Phanerozoic plumes may stay solid hampering assimilation of much H_2O within a short period of time (Sobolev et al., 2016). As most Phanerozoic plumes have similar mantle potential temperatures (consistently lower than Archean plumes; Herzberg & Gazel, 2009; Sobolev et al., 2016), it means that the different H_2O contents in plume-related OIBs are not caused by entraining variable amounts of materials from the transition zone during plume upwelling.

There is a wide consensus that variable chemical and isotopic compositions of plume-related OIBs reflect notable compositional heterogeneity of the deep mantle (Hofmann, 1997; White, 2015). As accumulative geophysical observations and numerical models propose that most mantle plumes feeding OIBs are rooted in the LLSVPs, the significant variations in H_2O contents and H_2O/Ce ratios in primary melts and mantle sources for diverse plume-induced OIBs could indicate heterogeneous distribution of H_2O in the LLSVPs (Figures 6a, b). Additionally, geophysical observations have also revealed heterogeneity inside individual LLSVPs (e.g., Garnero et al., 2016).

5.4. More hydrous African LLSVP

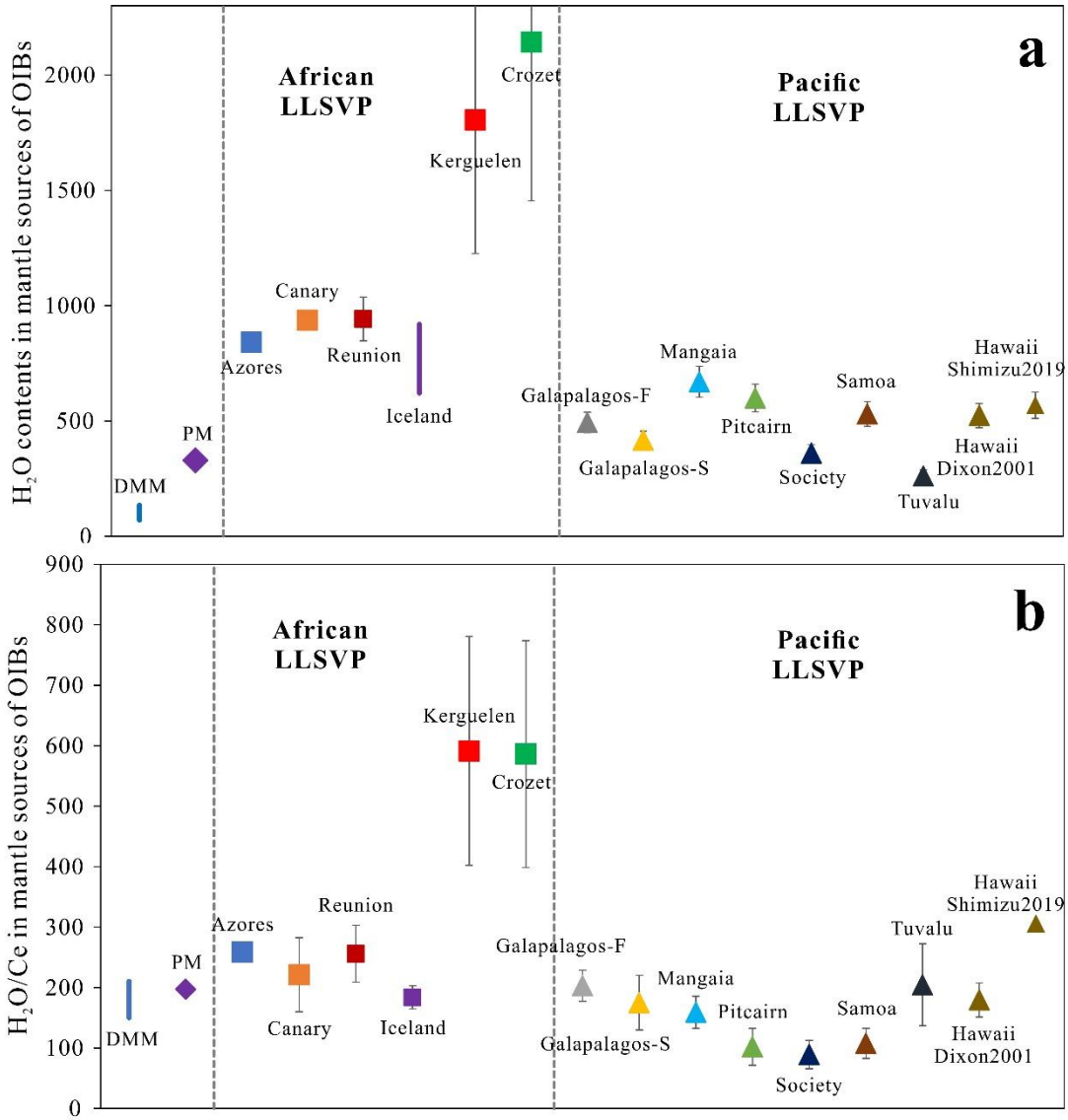

Figure 6 Estimated H_2O contents (a) and H_2O/Ce ratios (b) in the mantle sources of OIBs originally related to the African and Pacific LLSVPs. H_2O contents were estimated from the calculated H_2O contents of primary melts using the batch melting model and H_2O partition coefficient of 0.0085 (Table 1; the calculation details are shown in the supporting information). H_2O/Ce ratios in melts can represent those of their mantle sources. The H_2O contents and H_2O/Ce ratios in the depleted MORB source mantle (DMM) and primitive mantle (PM) were adopted from Bizimis and Peslier (2015). The H_2O content and H_2O/Ce ratio in the source of basalts originating from the Iceland plume are adopted from Nichols et al. (2002) and Hartley et al. (2015), respectively. The H_2O content and H_2O/Ce ratio in the Hawaii plume estimated from basaltic glasses by Dixon and Clague (2001) and Shimizu et al. (2019) were shown separately, named as 'Hawaii Dixon2001' and 'Hawaii Shimizu2019', respectively. The H_2O

content and H_2O/Ce ratio of the mantle source for 'Hawaii shimizu2019' were estimated from the glass with the highest H_2O content and H_2O/Ce ratio reported by Shimizu et al. (2019). Shimizu et al. (2019) only analyzed three glasses and their compositions and H_2O contents display significant variations.

The existence of the Kerguelen and Crozet mantle plumes has been repeatedly demonstrated by diverse geophysical observations (e.g., French & Romanowicz, 2015; Marignier et al., 2020; Montelli et al., 2004, 2006) and is consistent with primitive He isotopic compositions of Cenozoic basalts (Breton et al., 2013; Doucet et al., 2006). Both mantle plumes are deeply rooted at the base of the mantle and the induced hotspots are geographically associated with the African LLSVP (e.g., French & Romanowicz, 2015; Jackson et al., 2018; Montelli et al., 2006). Together with basalts generated by other plumes originating from the LLSVPs, we can catch a glimpse into the H_2O distribution in the African and Pacific LLSVPs.

As shown in Section 5.3, we have compiled the data of the plume-induced OIBs representing different mantle end-members as many as possible (Dataset S2). For the African LLSVP, the data for St. Helena basalts, compositionally close to the HIMU endmember component, is absent. Only one H_2O content value for a glass from St. Helena was reported (Kendrick et al., 2017), while its bulk rock MgO content is 2.8 wt.%, indicating that it has too strongly evolved to recover the H_2O content in the mantle source. The data shows that irrespective of the geochemical affinity to different mantle endmembers, OIBs associated with the African LLSVP form a trend extending to higher H_2O contents compared with those associated with the Pacific LLSVP (Figure 5b). For the latter, H_2O contents do not increase with Ce (especially in samples with Ce concentrations higher than 80 ppm; Figure 5b). In comparison, the H_2O contents in the mantle sources of OIBs from African LLSVP were estimated to range from 620 to 2144 ppm, which are systematically higher than those

401 estimated for OIBs from the Pacific LLSVP (262-671 ppm; Table 1; Figure 6a; the calculation
402 details are shown in the supporting information). The H_2O/Ce ratios of the Crozet and Kerguelen
403 basalts are also higher than those of the Pacific LLSVP, the depleted MORB source mantle, and the
404 primitive mantle (Figure 6b). Overall, the H_2O/Ce ratios of OIBs from the African LLSVP are close
405 to or higher than the upper boundary of the H_2O/Ce ratio range for the OIBs from the Pacific LLSVP
406 (184-592 versus 89-306; Figure 6b).

407 Furthermore, remarkably high H_2O/Ce ratios have been observed in the North (253 ± 33, Dixon et
408 al., 2002) and equatorial (205-405, mostly higher than 250, Le Voyer et al., 2015) Mid-Atlantic
409 MORBs imprinted by mantle plumes, which are rooted in the African LLSVP. The Afar mantle
410 plume, another 'primary plume' detected by French and Romanowicz (2015), is also deeply
411 associated with the African LLSVP and underlies the African continent. However, the H_2O contents
412 of Afar plume-related basalts have never been studied so far, but geophysical observations indicate
413 that the lower mantle source of the Afar plume is enriched in volatiles (Thompson et al., 2015). All
414 these observations indicate that the African LLSVP is more hydrous than the antipodal Pacific
415 LLSVP.

416 **5.5. Implications for different formation histories for the LLSVPs**

417 Geophysical observations and numerical modeling support the view that the LLSVPs are piles of
418 accumulative dense mantle materials, the origin of which has been proposed to be Fe-rich remnants
419 of ancient differentiation in the mantle or continuous accumulation of subducted oceanic crust
420 (Garnero et al., 2016). Lee et al. (2010) suggested that the primordial Fe-rich by-products of Archean
421 differentiation have FOZO-like geochemical characteristics. However, most OIBs geographically

422 associated with both LLSVPs deviate from the DMM-FOZO trend in the H_2O versus Ce plot (Figure
423 5b; Shimizu et al., 2019). Compared with the primitive mantle, the H_2O content in the mantle
424 sources of all the OIBs and H_2O/Ce ratios of most OIBs from the African LLSVP are significantly
425 higher, whereas those of the Pacific are mostly lower (Figures 6a, b). The observed features of H_2O
426 distribution in LLSVPs may not have resulted from ancient differentiation.

427 High-P-T experiments have shown that hydrous minerals have the ability to transport large amounts
428 of H_2O by subduction into the bottom of the lower mantle (e.g., Nishi et al., 2014). Subducted slabs
429 may experience variable extents of dehydration during their downwelling into and residence in the
430 lower mantle (e.g., Kendrick et al., 2017; Workman et al., 2006), which was applied to explain the
431 contrasting H_2O contents in diverse OIBs (e.g., Cabral et al., 2014; Dixon et al., 2002; Kendrick et
432 al., 2017). The distinct H_2O contents in these two LLSVPs might be indictive of different extents of
433 dehydration in subducted materials incorporated into individual LLSVPs. The dehydration extent
434 of subducting slabs depends on the conditions of the slabs and the subduction environment (e.g.,
435 van Keken et al., 2011). Huge amounts of subducted oceanic crust underwent dehydration to
436 different degrees and accumulated at the base of the lower mantle to form the LLSVPs, indicating
437 that the massive subduction responsible for the generation of the African and Pacific LLSVPs may
438 have occurred in different geological periods. White (2015) has proposed that the two LLSVPs may
439 be compositionally distinct, as indicated by the presence of ubiquitous isotopic DUPAL anomalies
440 in basalts from the south Atlantic and Indian Oceans, but not in basalts from the south Pacific Ocean.
441 In addition, the cluster analysis of seismic tomographic models reveals that the African and Pacific
442 LLSVPs have different shapes and vertical extents, which strongly depend on the viscosity of deep
443 mantle materials (Cottaar & Lekic, 2016; Deschamps & Tackley, 2008). Because H_2O can

444 significantly affect the rheological properties of mantle minerals, the differences in the H_2O contents
445 in the two LLSVPs may be an important factor in accounting for their seismic differences.

446 Our observations, that the two LLSVPs have distinct H_2O contents and H_2O/Ce ratios, may imply
447 that the formation and evolution should be different for the African and Pacific LLSVPs. Numerical
448 models show that the formation of LLSVPs can be related to tectonic processes in the last 120 Ma
449 (e.g., McNamara & Zhong, 2005) or super-continental cycles (e.g., Doucet et al., 2020; Li & Zhong,
450 2009; Zhang et al., 2010). It has been suggested that the structure of the lower mantle beneath Africa
451 may have been generated as the result of mantle upwelling corresponding to the subduction around
452 the supercontinent Pangea (Zhang et al., 2010). In contrast, the thermochemical piles responsible
453 for the Pacific LLSVP could have been emplaced before the assembly of Pangea, perhaps during
454 the lifetime of the supercontinent Rodinia or after the breakup of Rodinia as the upwelling system
455 driving the assembly of Pangea (Doucet et al. 2020; Li & Zhong, 2009).

456 **6. Conclusions**

457 H_2O contents in hotspots-related basalts fed by mantle plumes, deeply rooted in the African and
458 Pacific LLSVPs, were used to obtain information on the H_2O distribution in these two LLSVPs. The
459 H_2O concentrations in the calculated primary melts of Cenozoic basalts, unmodified melting
460 products of the Kerguelen and Crozet mantle plumes, were estimated to be 1.68 ± 0.54 wt.% and
461 3.69 ± 1.18 wt.%, respectively. Combined with melting models, the H_2O contents of the Kerguelen
462 and Crozet mantle plumes were estimated to be 1805 ± 579 ppm and 2144 ± 690 ppm for the
463 Kerguelen and Crozet mantle plumes, respectively, giving an indication of the H_2O distribution
464 inside the African LLSVP. We compiled H_2O content data from worldwide plume-fed OIBs and

back-calculated the H_2O contents in their primary melts and mantle sources, with the results displaying large variations among plume-fed OIBs, even for basalts geographically associated with a single LLSVP. We conclude that the African LLSVP is more enriched in H_2O and has higher H_2O/Ce ratios compared with the Pacific LLSVP. Incorporation of subducted oceanic crust with variable extents of dehydration during its downwelling can be responsible for the heterogeneous distribution of H_2O within individual LLSVPs and the distinct H_2O contents and H_2O/Ce ratios between the African and Pacific LLSVPs. The present observations suggest that these two LLSVPs have different formation and evolution histories.

		Compositions of OIBs						Primary water content (wt.%)	Errors	Water content in mantle source				Water content in mantle source		
		H_2O (wt.%)	Errors*	MgO (wt.%)&	Olivine addition§	H_2O/Ce£	Errors$			Batch melting				Fractional melting		
	OIBs									D = 0.0085#	Errors	D = 0.0046	D = 0.011	D = 0.0085	D = 0.0046	D = 0.011
African LLSVP	Azores	1.83	0.18	6.51	0.21	259.12	33.51	1.45	0.14	841.20	84.53	787.53	875.60	725.97	724.24	724.23
	Canary	2.27	0.09	7.33	0.29	221.30	61.20	1.61	0.06	936.70	37.29	876.94	975.01	808.39	806.47	806.46
	Reunion	1.01	0.10	11.06	0.13	256.16	47.02	0.88	0.09	942.71	94.51	911.97	962.41	875.72	875.71	875.71
	Iceland **					184.00	19.00			620-920						
	Kerguelen &&	2.02	0.65		0.17	591.57	189.30	1.68	0.54	1804.86	579.00	1746.01	1842.58	1676.61	1676.60	1676.60
	Crozet	3.97	1.27		0.07	586.22	187.59	3.69	1.18	2144.19	689.51	2007.39	2231.87	1850.48	1846.08	1846.05
Pacific LLSVP	Galapalagos_F§§	0.60	0.05	7.44	0.23	203.06	25.62	0.46	0.04	493.20	44.50	477.12	503.51	458.15	458.15	458.15
	Galapalagos_S§§	0.50	0.05	7.06	0.23	175.19	45.26	0.39	0.03	417.77	37.69	404.15	426.50	388.08	388.08	388.08
	Mangaia	1.37	0.14	10.80	0.16	159.07	26.41	1.15	0.12	670.61	67.39	627.83	698.04	578.75	577.37	577.37
	Pitcairn	0.79	0.08	5.94	0.29	101.98	30.55	0.56	0.06	599.99	60.15	580.42	612.53	557.35	557.35	557.35
	Society	0.88	0.09	6.93	0.29	89.19	23.49	0.62	0.06	360.79	36.26	337.77	375.55	311.37	310.63	310.63
	Samoa	1.17	0.12	8.78	0.22	107.71	24.72	0.91	0.09	529.99	53.26	496.18	551.67	457.40	456.31	456.30
	Tuvalu	0.59	0.06	8.12	0.24	204.64	67.62	0.45	0.05	261.63	26.29	244.93	272.32	225.79	225.25	225.25
	Hawaii££	0.64	0.06	8.25	0.24	179.54	28.16	0.49	0.05	523.61	52.49	506.54	534.55	486.40	486.40	486.40
	Hawaii$$	1.44	0.14	7.52	0.32	305.67		0.98	0.10	567.97	57.08	531.74	591.20	490.17	489.01	489.00

Table 1 Estimated water contents in primary melts and mantle sources of global OIBs. The details about the calculation procedure are shown in the supporting information. The references for the compositions and water contents of individual OIBs are listed in the caption of Figure 5. The data of melt inclusions or glasses with the highest MgO contents reported by literatures for individual hotspot-related OIBs were applied to retrieve the compositions and water contents of corresponding primary melts and sources. * The errors of water contents for OIBs are estimated

from the analytical errors reported in the literatures. [&] The highest MgO contents of melt inclusions or glasses adopted from referenced literatures for individual OIBs. [£] We use the average H_2O/Ce ratios for all the melt inclusions or glasses (preserving initial information) in our referenced literatures to represent the H_2O/Ce ratios of corresponding primary melts. [§] The proportions of olivine addition to the highest-MgO OIB compositions for primary melt compositions. [$] The standard deviations for averaging H_2O/Ce ratios of all the melt inclusions or glasses. [#] D is the partition coefficient of H_2O between the source and primary melt. The choose of partition coefficients is discussed in detail in the supporting information. [**] The H_2O content and H_2O/Ce ratio in the source of the Iceland hotspot are not calculated in this study, and are just adopted from Nichols et al. (2002) and Hartley et al. (2015). [&&] Water contents in Kerguelen and Crozet basalts are estimated for melts equilibrated with Cpx phenocrysts (Mg# higher than 85). The errors are estimated from the uncertainty of 32% for the whole calculation procedure. Ce concentrations are from the bulk rock measurements. [§§] For the Galapalago hotspot, only H_2O contents in basalts with $^3He/^4He$ >8 were taken into consideration (two groups Fernandina and Sierra Negra, suffixed by 'F' and 'S'; Peterson et al., 2017). [ŁŁ] The H_2O content and H_2O/Ce ratio in the Hawaii plume were estimated from basaltic glasses studied by Dixon and Clague (2001). [$$] The H_2O content and H_2O/Ce ratio in the Hawaii plume were estimated from basaltic glasses studied by Shimizu et al. (2019).

Acknowledgements

This study was supported by the Strategic Priority Research Program (B) of Chinese Academy of Sciences (grant no. XDB18000000) and the National Natural Science Foundation of China (grant nos. 41702046 and 41630205). The data related to this study are available on the public repository (https://doi.org/10.6084/m9.figshare.13347137.v1).

References

Aubaud, C., Hauri, E. H., & Hirschmann, M. M. (2004). Hydrogen partition coefficients between nominally anhydrous minerals and basaltic melts. *Geophys. Res. Lett., 31*, L20611. https://doi.org/10.1029/2004GL021341

Bell, D. R., Ihinger, P. D., & Rossman, G. R. (1995). Quantitative analysis of trace OH in garnet and pyroxenes. *Am. Mineral., 80*, 465-474. https://doi.org/10.2138/am-1995-5-608

Bell, D. R., Rossman, G. R., Maldener, J., Endisch, D. H., & Rauch, F. (2003). Hydroxide in olivine: A quantitative determination of the absolute amount and calibration of the IR spectrum. *J. Geophys. Res., 108*, 2105. https://doi.org/10.1029/2001JB000679

Bizimis M., & Peslier A. H. (2015). Water in Hawaiian garnet pyroxenites: Implications for water heterogeneity in the mantle. *Chem. Geol., 397*, 61-75. https://doi.org/10.1016/j.chemgeo.2015.01.008

Brandenburg, J. P., & van Keken, P. E. (2007). Deep storage of oceanic crust in a vigorously convecting mantle. *J. Geophys. Res., 112*, B06403. https://doi.org/10.1029/2006JB004813

Breton, T., Nauret, F., Pichat, S., Moine, B., Moreira, M., Rose-Koga, E. F., et al. (2013). Geochemical heterogeneities within the Crozet hotspot. *Earth Planet. Sci. Lett., 376*, 126-136. https://doi.org/10.1016/j.epsl.2013.06.020

Cabral, R. A., Jackson, M. G., Koga, K. T., Rosekoga, E. F., Hauri, E. H., Whitehouse, M. J., et al. (2014). Volatile cycling of H_2O, CO_2, F, and Cl in the HIMU mantle: A new window provided by melt inclusions from oceanic hot spot lavas at Mangaia, Cook Islands. *Geochem. Geophys. Geosyst., 15*, 4445-4467. https://doi.org/10.1002/2014gc005473

Coffin, M. F., Pringle, M. S., Duncan, R. A., Gladczenko, T. P., Storey, M., Müller, R. D., & Gahagan, L. A. (2002). Kerguelen hotspot magma output since 130 Ma. *J. Petrol., 43*, 1121-1139. https://doi.org/10.1093/petrology/43.7.1121

Cottaar, S., & Lekic, V. (2016). Morphology of Seismically Slow Lower Mantle Structures. *Geophys. J. Inter., 207*, 1122-1136. https://doi.org/10.1093/gji/ggw324

Deschamps, F., & Tackley, P. J. (2008). Searching for models of thermo-chemical convection that explain probabilistic tomography: I. Principles and influence of rheological parameters. *Phys. Earth Planet. Int., 171*, 357-373. https://doi.org/10.1016/j.pepi.2009.03.012

Dixon, J. E., & Clague, D. A. (2001). Volatiles in Basaltic Glasses from Loihi Seamount, Hawaii: Evidence for a Relatively Dry Plume Component. *J. Petrol., 42*, 627-654. https://doi.org/10.1093/petrology/42.3.627

Dixon, J. E., Leist, L., Langmuir, C. H., & Schilling, J. (2002). Recycled dehydrated lithosphere observed in plume-influenced mid-ocean-ridge basalt. *Nature, 420*, 385-389. https://doi.org/10.1038/nature01215

Doucet, L. S., Li, Z. X., El Dien, H. G., Pourteau, A., Murphy, B., Collins, W. J., et al. (2020). Distinct formation history for deep-mantle domains reflected in geochemical differences. *Nat. Geosci., 13*, 511-515. https://doi.org/10.1038/s41561-020-0599-9

Doucet, S., Moreira, M., Weis, D., Scoates, J. S., Giret, A., Allegre, C. J. (2006). Primitive neon and helium isotopic compositions of high-MgO basalts from the Kerguelen Archipelago, Indian Ocean. *Earth Planet. Sci. Lett., 241*, 65-79. https://doi.org/10.1016/j.epsl.2005.10.025

Doucet, S., Scoates, J. S., Weis, D., & Giret, A. (2005). Constraining the components of the Kerguelen mantle plume: A Hf-Pb-Sr-Nd isotopic study of picrites and high-MgO basalts from the Kerguelen Archipelago. *Geochem. Geophys. Geosyst., 6*, Q04007. https://doi.org/10.1029/2004gc000806

Dunstan, L. P., Gramlich, J. W., & Barnes, I. L. (1980). Absolute isotopic abundance and the atomic weight of a reference sample of thallium. *J. Res. Nat. Bureau Stand., 85*, 1–10. https://doi.org/10.6028/jres.085.001

527 French, S. W., & Romanowicz, B. (2015). Broad plumes rooted at the base of the earth's mantle beneath major hotspots. *Nature, 525*, 95-
528 99. https://doi.org/95-99. 10.1038/nature14876

529 Frey, F. A., Coffin, M. F., Wallce, P. J., Weis, D., Zhao, X., Wise Jr. S. W., et al. (2000a). Origin and evolution of a submarine large igneous
530 province: the Kerguelen Plateau and Broken Ridge, southern Indian Ocean. *Earth Planet. Sci. Lett., 176*, 73-89.
531 https://doi.org/10.1016/S0012-821X(99)00315-5

532 Frey, F. A., Weis, D., Yang, H. J., Nicolaysen, K., Leyrit, H., & Giret, A. (2000b). Temporal geochemical trends in Kerguelen Archipelago
533 basalts: evidence for decreasing magma supply from the Kerguelen Plume. *Chem. Geol., 164*, 61-80. https://doi.org/10.1016/S0009-
534 2541(99)00144-8

535 Gale, A., Dalton, C. A., Langmuir, C. H., Su, Y., & Schilling, J. (2013). The mean composition of ocean ridge basalts. Geochem.
536 *Geophys. Geosyst., 14*, 489-518. https://doi.org/10.1029/2012GC004334

537 Garnero, E. J., McNamara, A. K., & Shim, S. H. (2016). Continent-sized anomalous zones with low seismic velocity at the base of Earth's
538 mantle. *Nat. Geosci., 9*, 481-489. https://doi.org/10.1038/ngeo2733

539 Hartley, M. E., Neave, D. A., Maclennan, J., Edmonds, M., & Thordarson, T. (2015). Diffusive over-hydration of olivine-hosted melt
540 inclusions. *Earth Planet. Sci. Lett., 425*, 168-178. https://doi.org/10.1016/j.epsl.2015.06.008

541 Herzberg, C., & Gazel, E. (2009). Petrological evidence for secular cooling in mantle plumes. *Nature, 458*, 619-622.
542 https://doi.org/10.1038/nature07857

543 Hirschmann, M. M., Tenner, T. J., Aubaud, C., & Withers, A. C. (2009). Dehydration melting of nominally anhydrous mantle: The primacy
544 of partitioning. *Phys. Earth Planet. Int., 176*, 54-68. https://doi.org/10.1016/j.pepi.2009.04.001

545 Hofmann, A. W. (1997). Mantle geochemistry: the message from oceanic volcanism. *Nature, 385*, 219-229.
546 https://doi.org/10.1038/385219a0

547 Hofmann, A.W., Jochum, K.P., Seufert, M., & White, W.M. (1986). Nb and Pb in oceanic basalts: New constraints on mantle evolution.

548 *Earth Planet. Sci. Lett., 79*, 33-45. https://doi.org/10.1016/0012-821X(86)90038-5

549 Homrighausen, S., Hoernle, K., Zhou, H., Geldmacher, J., Wartho, J-A., Hauff, F., et al. (2020). Paired EMI-HIMU hotspots in the South
550 Atlantic-Starting plume heads trigger compositionally distinct secondary plumes? *Sci. Adv., 6*, eaba0282.
551 https://doi.org/10.1126/sciadv.aba0282

552 Hsieh, W. P., Ishii, T., Chao, K. H., Tsuchiya, J., Deschamps, F., & Ohtani, E. (2020). Spin transition of iron in δ‐(Al,Fe)OOH induces
553 thermal anomalies in Earth's lower mantle. *Geophys. Res. Lett., 47*, 087036. https://doi.org/10.1029/2020GL087036

554 Huang, S., Hall, P. S., & Jackson, M. G. (2011). Geochemical zoning of volcanic chains associated with Pacific hotspots. *Nat. Geosci., 4*,
555 874-878. https://doi.org/10.1038/ngeo1263

556 Jackson, M. G., Koga, K. T., Price, A. A., Konter, J. G., Koppers, A. A., Finlayson, V., et al. (2015). Deeply dredged submarine HIMU
557 glasses from the Tuvalu Islands, Polynesia: Implications for volatile budgets of recycled oceanic crust. *Geochem. Geophys. Geosyst.,*
558 *16*, 3210-3234. https://doi.org/10.1002/2015GC005966

559 Jackson, M. G., Becker, T. W., & Konter, J. G. (2018). Geochemistry and distribution of recycled domains in the mantle inferred from Nd
560 and Pb isotopes in oceanic hot spots: Implications for storage in the Large Low Shear Wave Velocity Provinces. *Geochem. Geophys.*
561 *Geosyst., 19*, 3496-3519. https://doi.org/10.1029/2018GC007552

562 Kendrick, M. A., Jackson, M. G., Kent, A. J., Hauri, E. H., Wallace, P. J., & Woodhead, J. D. (2014). Contrasting behaviours of CO_2, S,
563 H_2O and halogens, F, Cl, Br, and I in enriched-mantle melts from Pitcairn and Society seamounts. *Chem. Geol., 370*, 69-81.
564 https://doi.org/10.1016/j.chemgeo.2014.01.019

565 Kendrick, M. A., Jackson, M. G., Hauri, E. H., & Phillips, D. (2015). The halogen, F, Cl, Br, I and H_2O systematics of Samoan lavas:
566 Assimilated-seawater, EM2 and high-$^3He/^4He$ components. Earth Planet. Sci. Lett. 410, 197-209.
567 https://doi.org/10.1016/j.epsl.2014.11.026

Kendrick, M. A., Hemond, C., Kamenetsky, V. S., Danyushevsky, L. V., Devey, C. W., Rodemann, T., et al. (2017). Seawater cycled throughout Earth's mantle in partially serpentinized lithosphere. *Nat. Geosci., 10*, 222-228. https://doi.org/10.1038/ngeo2902

Kuritani, T., & Nakamura, E. (2002). Precise isotope analysis of nanogram-level Pb for natural rock samples without use of double spikes. *Chem. Geol., 186*, 31-43. https://doi.org/10.1016/S0009-2541(02)00004-9

Kuritani, T., & Nakamura, E. (2003). Highly precise and accurate isotopic analysis of small amounts of Pb using ^{205}Pb-^{204}Pb and ^{207}Pb-^{204}Pb, two double spikes. *J. Analytical Atomic Spectro., 18*, 1464-1470. https://doi.org/10.1039/B310294G

Kuritani, T., Nakagawa, M., Nishimoto, J., Yokoyama, T., & Miyamoto, T. (2020). Magma plumbing system for the Millennium Eruption at Changbaishan volcano, China: constraints from whole-rock U-Th disequilibrium. *Lithos, 366-367*, 105564. https://doi.org/10.1016/j.lithos.2020.105564

Labrosse, S., Hernlund, J. W., & Coltice, N. (2007). A crystallizing dense magma ocean at the base of the Earth's mantle. *Nature, 450*, 866-869. https://doi.org/10.1038/nature06355

Langmuir, C. H., Vocke, R. D., Hanson, G. N., & Hart, S. R. (1978). A general mixing equation with applications to Icelandic basalts. *Earth Planet. Sci. Lett., 37*, 380-392. https://doi.org/10.1016/0012-821X(78)90053-5

Lee, C. T. A., Luffi, P., Hoink, T., Li, J., Dasgupta, R., & Hernlund, J. (2010). Upside-down differentiation and generation of a 'primordial' lower mantle. *Nature, 463*, 930–933. https://doi.org/10.1038/nature08824

Le Voyer, M., Cottrell, E., Kelley, K.A., Brounce, M., & Hauri, E. H. (2015). The effect of primary versus secondary processes on the volatile content of MORB glasses: An example from the equatorial Mid-Atlantic Ridge, 5°N-3°S. *J. Geophys. Res., 120*, 125-144. https://doi.org/10.1002/2014JB011160

Li, M., McNamara, A. K., & Garnero, E. J. (2014). Chemical complexity of hotspots caused by cycling oceanic crust through mantle reservoirs. *Nat. Geosci., 7*, 366-370. https://doi.org/10.1038/ngeo2120

588 Li, Z., & Zhong, S. (2009). Supercontinent-superplume coupling, true polar wander and plume mobility: Plate dominance in whole-
589 mantle tectonics. *Phys. Earth Planet. Int., 176*, 143-156. https://doi.org/10.1016/j.pepi.2009.05.004

590 Li, W., Jin, Z., Li, H., & Tao, C. (2017). High water content in primitive mid-ocean ridge basalt from Southwest Indian Ridge, 51.56ºE:
591 Implications for recycled hydrous component in the mantle. *J. Earth Sci., 28*, 411-421. https://doi.org/10.1007/s12583-017-0731-y

592 Liu, Y., Hu, Z., Gao, S., Günther, D., Xu, J., Gao, C., & Chen, H. (2008). In situ analysis of major and trace elements of anhydrous
593 minerals by LA-ICP-MS without applying an internal standard. *Chem. Geol., 257*, 34-43.
594 https://doi.org/10.1016/j.chemgeo.2008.08.004

595 Liu, J., Xia, Q.K., Deloule, E., Ingrin, J., Chen, H., & Feng, M. (2015). Water content and oxygen isotopic composition of alkali basalts
596 from the Taihang Mountains, China: Recycled oceanic components in the mantle source. *J. Petrol., 56*, 681-702.
597 https://doi.org/10.1093/petrology/egv013

598 Lloyd, A. S., Elizabeth, F., Philipp, R., Hauri, E. H., Jicha, B. R., & Terry, P. (2016). An assessment of clinopyroxene as a recorder of
599 magmatic water and magma ascent rate. *J. Petrol., 57*, 1865-1886. https://doi.org/10.1093/petrology/egw058

600 Longpré, M., Stix, J., Klügel, A., & Shimizu, N. (2017). Mantle to surface degassing of carbon- and sulphur-rich alkaline magma at El
601 Hierro, Canary Islands. *Earth Planet. Sci. Lett., 460*, 268-280. https://doi.org/10.1016/j.epsl.2016.11.043

602 Marignier, A., Ferreira, A. M. G., & Kitching, T. (2020). The probability of mantle plumes in global tomographic models. *Geochem.*
603 *Geophys. Geosyst., 21*, e2020GC009276. https://doi.org/10.1029/2020GC009276

604 McDonough, W. F., & Sun, S. S. (1995). The composition of the Earth. *Chem. Geol., 120*, 223-253. https://doi.org/10.1016/0009-
605 2541(94)00140-4

606 McNamara, A. K., & Zhong, S. (2005). Thermochemical structures beneath Africa and the Pacific Ocean. *Nature, 437*, 1136-1139.
607 https://doi.org/10.1038/nature04066

608 Métrich, N., Zanon, V., Creon, L., Hildenbrand, A., Moreira, M., & Marques, F. O. (2014). Is the 'Azores hotspot' a wetspot? Insights
609 from the geochemistry of fluid and melt inclusions in olivine of Pico basalts. *J. Petrol., 55*, 377-393.
610 https://doi.org/10.1093/petrology/egt071

611 Montelli, R., Nolet, G., Dahlen, F. A., & Masters, G. (2006). A catalogue of deep mantle plumes: New results from finite-frequency
612 tomography. *Geochem. Geophys. Geosyst., 7*, Q11007. https://doi.org/10.1029/2006GC001248

613 Montelli, R., Nolet, G., Dahlen, F. A., Masters, G., Engdahl, E. R., & Hung, S. H. (2004). Finite-frequency tomography reveals a variety
614 of plumes in the mantle. *Science, 303*, 338-343. https://doi.org/10.1126/science.1092485

615 Mulyukova, E., Steinberger, B., Dabrowski, M., & Sobolev, S. V. (2015). Survival of LLSVPs for billions of years in a vigorously
616 convecting mantle: Replenishment and destruction of chemical anomaly. *J. Geophys. Res., 120*, 3824-3847.
617 https://doi.org/10.1002/2014JB011688

618 Nakagawa, T., Nakakuki, T., & Iwamori, H. (2015). Water circulation and global mantle dynamics: Insight from numerical modeling.
619 *Geochem. Geophys. Geosyst., 16*, 1449-1464. 1 https://doi.org/0.1002/2014GC005701

620 Nichols, A. R. L., Carroll, M. R., & Höskuldsson, Á. (2002). Is the Iceland hot spot also wet? Evidence from the water contents of
621 undegassed submarine and subglacial pillow basalts. *Earth Planet. Sci. Lett., 202*, 77-87. https://doi.org/10.1016/S0012-
622 821X(02)00758-6

623 Nishi, M., Irifune, T., Tsuchiya, J., Tange, Y., Nishihara, Y., Fujino, K., & Higo, Y. (2014). Stability of hydrous silicate at high pressures
624 and water transport to the deep lower mantle. *Nat. Geosci., 7*, 224-227. https://doi.org/10.1038/ngeo2074

625 Noguchi, T., Shinjo, R., Ito, M., Takada, J., & Oomori, T. (2011). Barite geochemistry from hydrothermal chimneys of the Okinawa
626 Trough: insight into chimney formation and fluid/sediment interaction. *J. Miner. Petrol. Sci., 106*, 26-35.
627 https://doi.org/10.2465/jmps.090825

Nomura, R., Hirose, K., Uesugi, K., Ohishi, Y., Tsuchiyama, A., Miyake, A., & Ueno, Y. (2014). Low core-mantle boundary temperature inferred from the solidus of pyrolite. *Science, 343*, 522-525. https://doi.org/10.1126/science.1248186

O'Leary, J. A., Gaetani, G. A., & Hauri, E. H. (2010). The effect of tetrahedral Al^{3+} on the partitioning of water between clinopyroxene and silicate melt. *Earth Planet. Sci. Lett., 297*, 111-120. https://doi.org/10.1016/j.epsl.2010.06.011

Peterson, M., Saal, A. E., Kurz, M. D., Hauri, E. H., Blusztajn, J., Harpp, K. S., et al. (2017). Submarine basaltic glasses from the Galapagos Archipelago: Determining the volatile budget of the mantle plume. *J. Petrol., 58*, 1419-1450. https://doi.org/10.1093/petrology/egx059

Pin, C., & Zalduegui, J. F. S. (1997). Sequential separation of light rare-earth elements, thorium and uranium by miniaturized extraction chromatography: Application to isotopic analyses of silicate rocks. *Analytica Chimica Acta, 339*, 79-89. https://doi.org/10.1016/S0003-2670(96)00499-0

Pin, C., Briot, D., Bassin, C., & Poitrasson, F. (1994). Concomitant separation of strontium and samarium-neodymium for isotopic analysis in silicate samples, based on specific extraction chromatography. *Analytica Chimica Acta, 298*, 209-217. https://doi.org/10.1016/0003-2670(94)00274-6

Sauter, D., Cannat, M., Meyzen, C., Bezos, A., Patriat, P., Humler, E., & Debayle, E. (2009). Propagation of a melting anomaly along the ultraslow Southwest Indian Ridge between 46°E and 52°20′E: interaction with the Crozet hotspot? *Geophys. Res. Lett., 179*, 687-699. https://doi.org/10.1111/j.1365-246X.2009.04308.x

Shaw, D. M. (1970). Trace element fractionation during anatexis. *Geochim. Cosmochim. Acta, 34*, 237-243. https://doi.org/10.1016/0016-7037(70)90009-8

Shimizu, K., Ito, M., Chang, Q., Miyazaki, T., Ueki, K., Toyama, C., et al. (2019). Identifying volatile mantle trend with the water–fluorine–cerium systematics of basaltic glass. *Chem. Geol., 522*, 283-294. https://doi.org/10.1016/j.chemgeo.2019.06.014

Sobolev, A. V., Asafov, E., Gurenko, A. A., Arndt, N.T., Batanova, V. G., Portnyagin, M., et al. (2016). Komatiites reveal a hydrous Archaean deep-mantle reservoir. *Nature, 531*, 628-632. https://doi.org/10.1038/nature17152

Sobolev, A. V., Hofmann, A. W., Kuzmin, D. V., Yaxley, G. M., Arndt, N. T., Chung, S. L., et al. (2007). The amount of recycled crust in sources of mantle-derived melts. *Science, 316*, 412-417. https://doi.org/10.1126/science.1138113

Thompson, D. A., Hammond, J. O. S., Kendall, J-M., Stuart, G. W., Helffrich, G., Keir, D., et al. (2015). Hydrous upwelling across the mantle transition zone beneath the Afar Triple Junction. *Geochem. Geophys. Geosyst., 16*, 834-846. https://doi.org/10.1002/2014GC005648

Thomson, A. R., Crichton, W. A., Brodholt, J. P., Wood, I. G., Siersch, N. C., Muir, J. M. R., et al. (2019). Seismic velocities of $CaSiO_3$ perovskite can explain LLSVPs in Earth's lower mantle. *Nature, 572*, 643-647. https://doi.org/10.1038/s41586-019-1483-x

Tian, Z., Liu, J., Xia, Q., Ingrin, J., Hao, Y., & Christophe, D. (2017). Water concentration profiles in natural mantle orthopyroxenes: A geochronometer for long annealing of xenoliths within magma. *Geology, 45*, 87-90. https://doi.org/10.1130/G38620.1

van Keken, P. E., Hacker, B. R., Syracuse, E. M., & Abers, G. (2011). Subduction factory: 4. Depth-dependent flux of H_2O from subducting slabs worldwide. *J. Geophys. Res., 116*, B01401. https://doi.org/10.1029/2010JB007922

Wallace, P. J. (2002). Volatiles in submarine basaltic glasses from the Northern Kerguelen Plateau, ODP Site 1140: Implications for source region compositions, magmatic processes, and plateau subsidence. *J. Petrol., 43*, 1311-1326. https://doi.org/10.1093/petrology/43.7.1311

Walowski, K. J., Kirstein, L. A., De Hoog, J. C. M., Elliott, T. R., Savov, I. P., & Jones, R. E. (2019). Investigating ocean island mantle source heterogeneity with boron isotopes in melt inclusions. *Earth Planet. Sci. Lett., 508*, 97-108. https://doi.org/10.1016/j.epsl.2018.12.005

Weis, D., & Frey, F. A. (2002). Submarine basalts of the Northern Kerguelen Plateau: Interaction between the Kerguelen plume and the Southeast Indian Ridge revealed at ODP Site 1140. *J. Petrol., 43*, 1287-1309. https://doi.org/10.1093/petrology/43.7.1287

669 Weis, D., Frey, F. A., Schlich, R., Schaming, M., Montigny, R., Damasceno, D., et al. (2002). Trace of the Kerguelen mantle plume:
670 Evidence from seamounts between the Kerguelen Archipelago and Heard Island, Indian Ocean. *Geochem. Geophys. Geosyst., 3*, 1-
671 27. https://doi.org/10.1029/2001GC000251

672 Weis, F. A., Skogby, H., Troll, V. R., Deegan, F. M., & Dahren, B. (2015). Magmatic water contents determined through clinopyroxene:
673 Examples from the Western Canary Islands, Spain. *Geochem. Geophys. Geosyst., 16*, 2127-2146.
674 https://doi.org/10.1002/2015GC005800

675 White, W. M. (2015). Isotopes, DUPAL, LLSVPs, and Anekantavada. *Chem. Geol., 419*, 10-28.
676 https://doi.org/10.1016/j.chemgeo.2015.09.026

677 Workman, R. K., Hauri, E., Hart, S. R., Wang, J., & Blusztajn, J. (2006). Volatile and trace elements in basaltic glasses from Samoa:
678 Implications for water distribution in the mantle. *Earth Planet. Sci. Lett., 241*, 932-951. https://doi.org/10.1016/j.epsl.2005.10.028

679 Xia, Q. K., Liu, J., Liu, S. C., Kovács, I., Feng, M., & Dang, L. (2013). High water content in Mesozoic primitive basalts of the North
680 China Craton and implications on the destruction of cratonic mantle lithosphere. *Earth Planet. Sci. Lett., 361*, 85-97.
681 https://doi.org/10.1016/j.epsl.2012.11.024

682 Xu, Y., Tang, W., Hui, H., Rudnick, R. L., Shang, S., & Zhang, Z. (2019). Reconciling the discrepancy between the dehydration rates in
683 mantle olivine and pyroxene during xenolith emplacement. *Geochim. Cosmochim. Acta, 267*, 179-195.
684 https://doi.org/10.1016/j.gca.2019.09.023

685 Zhang, N., Zhong, S., Leng, W., & Li, Z. X. (2010). A model for the evolution of the Earth's mantle structure since the Early Paleozoic. *J.*
686 *Geophys. Res., 115*, B06401. https://doi.org/10.1029/2009JB006896